Spin excitations in the antiferromagnet $NaNiO_2$

S. de Brion,[1] C. Darie,[2] M. Holzapfel,[1,*] D. Talbayev,[3] L. Mihály,[3,4] F. Simon,[5] A. Jánossy,[5] and G. Chouteau[1]
[1]*Grenoble High Magnetic Field Laboratory, CNRS, Boîte Postal 166, 38042 Grenoble, France*
[2]*Laboratoire de Cristallographie, CNRS, Boîte Postal 166, 38042 Grenoble, France*
[3]*Department of Physics, Stony Brook University, New York 11794-3800, USA*
[4]*Electron Transport Research Group of the Hungarian Academy of Science and Department of Physics, Budapest University of Technology and Economics, 1111 Budapest, Hungary*
[5]*Budapest University of Technology and Economics, Institute of Physics and Solids in Magnetic Fields Research Group of the Hungarian Academy of Sciences, P. O. Box 91, H-1521 Budapest, Hungary*
(Received 31 March 2006; published 2 March 2007)

In $NaNiO_2$, Ni^{3+} ions form a quasi-two-dimensional triangular lattice of $S=1/2$ spins. The magnetic order observed below 20 K has been described as an *A* type antiferromagnet with ferromagnetic layers weakly coupled antiferromagnetically. We studied the magnetic excitations with the electron spin resonance for frequencies $1-20\ cm^{-1}$, in magnetic fields up to 14 T. The bulk of the results are interpreted in terms of a phenomenological model involving biaxial anisotropy for the spins: a strong easy-plane term, and a weaker anisotropy within the plane.

DOI: 10.1103/PhysRevB.75.094402 PACS number(s): 76.50.+g, 71.27.+a, 75.30.Et, 71.70.−d

I. INTRODUCTION

A two-dimensional triangular network of magnetic ions interacting via an antiferromagnetic interaction is a well known geometrically frustrated system where unconventional magnetic properties are expected.[1] Usually, a long range magnetic order occurs at low enough temperature. For instance, in XCl_2 with X=Cr, Br, or in $ACrO_2$ with A=Li, Ag, Cu, or $CsCuCl_3$ the magnetic order is based on a 120° spin structure on the triangles. All these compounds have an easy plane or easy axis anisotropy together with Heisenberg type antiferromagnetic interactions. In other compounds, no magnetic order was detected so far ($NaCrO_2$, $KCrO_2$, $NaTiO_2$, $LiNiO_2$). The possibility of the orbital order competing with the spin order makes $LiNiO_2$ particularly interesting. In this compounds the Ni^{3+} ions have a spin $S=1/2$ and the orbital occupation is doubly degenerate: the e_g orbitals $|3z^2-r^2\rangle$ and $|x^2-y^2\rangle$, have the same energy unless the oxygen octahedron around the magnetic ion becomes elongated or compressed due to the Jahn-Teller effect.

Surprisingly, no orbital order has been observed in $LiNiO_2$. The absence of both orbital and magnetic order in this compound has been the subject of intense debate lately, both experimentally[2] and theoretically.[3] In particular, there is still a controversy on what are the relevant magnetic interactions within the triangular planes and to what extend this compound is magnetically frustrated. The comparison with the isomorphic $NaNiO_2$ is aimed at elucidating this unconventional behavior. In $NaNiO_2$ a ferrodistortive orbital order (a collective Jahn-Teller distortion) is observed below 480 K (Ref. 4) and a long range antiferromagnetic order appears below 20 K.[5] This magnetic order was first described as an *A* type antiferromagnet with ferromagnetic planes coupled antiferromagnetically.[5,6] The magnetic superlattice has indeed been observed recently in neutron diffraction measurements.[7] However, the description of the magnetic system with just two magnetic interactions (an antiferromagnetic J_{AF} between subsequent NiO planes and a ferromagnetic J_F within the planes) fails to describe the whole magnetic behavior, in particular the presence of three characteristic fields observed in the magnetization curve.[9] The direction of the spins measured by neutron diffraction is also unusual: they point toward the center of one of the triangles in the oxygen octahedron surrounding each Ni ion, at 100° from the Ni plane.[7] Moreover, a recent inelastic neutron study[8] has shown the presence of two branches in the magnetic excitations, one going to zero energy at the magnetic zone center, while the second being a dispersionless mode at $\simeq 0.7$ meV.

We have performed electron spin resonance measurements in magnetic fields up to 14 T on powder samples of $NaNiO_2$. We adopted and extended the model used to describe the magnon spectrum.[8] We find that the low field behavior of the system is characteristic of an "easy-plane" magnet, with a small anisotropy within the plane. The spin-flop transition is assigned to this latter anisotropy. At high fields all spins are aligned parallel and the saturation effects dominate the behavior. Although the model described here is generally successful, we also observed a spin resonance mode that remains unexplained. The possible implications for the magnetic interactions in $LiNiO_2$ are discussed.

II. EXPERIMENTS

The $NaNiO_2$ powdered sample was obtained following the procedure described elsewhere.[4] The monoclinic $C2/m$ crystal structure was checked by x-ray powder diffraction. The system is quasi-two-dimensional: The Ni-Ni interplane distance is large, 5.568 Å. Below the Jahn-Teller transition at 480 K the Ni^{3+} ions are arranged in a slightly distorted triangular network, with one short length and two longer ones (at room temperature, the Ni-Ni distances are 2.84 and 3.01 Å, respectively, compared to 2.96 Å at 565 K).[4] Also, the oxygen octahedra surrounding the nickel ions are elongated. Such a distortion favors the $|3z^2-r^2\rangle$ orbitals. Indeed, the electron spin resonance (ESR) spectra at 200 K have the

anisotropic shape typical of the $|3z^2-r^2\rangle$ orbitals, with $g^{\parallel}=2.03$ and $g^{\perp}=2.28$ for fields parallel and perpendicular to z, respectively.[4]

The magnetic behavior of our $NaNiO_2$ sample was the same as the one reported previously.[9] The magnetic susceptibility exhibits a Curie-Weiss behavior above 100 K. The Curie-Weiss temperature of $T_{CW}=36$ K reflects the predominance of ferromagnetic interactions. This is a noticeable difference compared to frustrated triangular compounds such as $LiCrO_2$. The effective magnetic moment (1.85 μ_B) is in agreement with the $|3z^2-r^2\rangle$ orbital configuration for the e_g electron in the low spin state of Ni^{3+} (spin $S=1/2$, average gyromagnetic factor $g_{av}=2.14$). The Néel temperature, observed as a peak in the susceptibility, is $T_N=20$ K. The magnetization curve in the ordered phase at 4 K presents two kinks at $H_{C0}=1.8$ T, $H_{C1}=8$ T, previously assigned to spin flop transitions, and the magnetization is fully saturated at $H_{sat}=13$ T.[9]

The electron spin resonance measurements were performed using two different techniques. Classical high frequency, high magnetic field ESR was used at fixed frequencies using Gunn diode oscillators and multipliers at 35, 75, 150, and 225 GHz, combined with a 9 T magnet at the Budapest University of Technology and Economics. Previous measurements at the Grenoble High Magnetic Field Laboratory have been described in Ref. 5.

Other measurements were performed by another method.[10,11] We used the far infrared facilities of the National Synchrotron Light Source in Brookhaven National Laboratory, at the U12 IR beamline, including a 14 T superconducting magnet (Oxford Instruments), and a Fourier transform infrared spectrometer (Sciencetech, SPS 200). We will present results obtained in the frequency range 3–20 cm^{-1} (90–600 GHz) at 4 K. The powdered sample was in a disk-shaped teflon container of 5 mm diameter and 1 mm thickness, in the center of the magnet. Light pipes were used to guide the infrared light from spectrometer to the sample, and the transmitted light was detected with a bolometer operating at 1.2 K temperature. The light propagated parallel to the static magnetic field. Spectra were recorded at fixed fields. The frequency resolution was selected at 0.2 cm^{-1}, much less than the width of the resonance lines. The upper frequency cutoff was adjusted to about 20 cm^{-1} with a Fluorogold filter of appropriate thickness. The lower cutoff was limited by the incident spectrum and the spectrometer performance. The signal to noise ratio was good down to 3 cm^{-1}, but there were strong minima in the incident light intensity around 3.7 and 4.6 cm^{-1}. We eliminated the experimental points at these minima without loosing the data around them, obtaining reliable signal down to 3 cm^{-1}. After averaging over several spectra (typically between two and four) and smoothing, the absorption spectrum at a given field was divided by a reference spectrum recorded at zero magnetic field, following the same procedure as described in Ref. 11.

III. RESULTS

First, we present the ESR results obtained with the classical ESR technique. A typical spectrum (the derivative of the absorption signal), recorded at 2.4 K at 75 GHz in the antiferromagnetic phase, has three resonance features (Fig. 1). The lines labeled (A), (B), and (C) are shifted from the paramagnetic $g=2$ line differently and they exhibit different temperature dependencies. Mode (A) has been already studied in Ref. 5 and was related to the spin flop field at 1.8 T. Mode (B) remains close to the paramagnetic line. Mode (C) consists of two close resonances which broaden with temperature and are hardly resolved above 6 K. Therefore only the first, larger intensity, resonance is plotted for the temperature dependence of mode (C). Below the phase transition temperature T_N, this mode behaves as the order parameter.

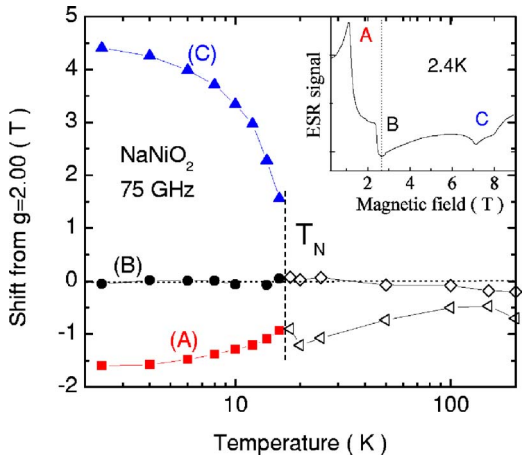

FIG. 1. (Color online) Shift of the resonance lines position from the paramagnetic line at 75 GHz as a function of temperature. Inset: typical ESR spectrum as a function of magnetic field recorded at 2.4 K. The dotted line corresponds to the paramagnetic line at $g=2$.

The paramagnetic line splitting at 200 K (empty symbols in Fig. 1) is due to the g factor anisotropy associated with the $|3z^2-r^2\rangle$ orbital occupation and has been discussed previously by Chappel *et al.*[4] We will discuss the paramagnetic state in a separate publication.[15]

The measurements were done on powder samples, and therefore the large line broadening seen in Fig. 1 is not surprising. For any given crystallite in the sample, the line position depends on the relative direction of external field and the crystallographic axes. Relatively sharp features appear in the spectrum because in the powder sample certain resonance frequencies (e.g., the highest and the lowest possible values) acquire large statistical weight. This effect is well known from the powder samples with significant g-factor anisotropy.

It is also important to notice that the presence of three lines in the spectrum at finite field does not necessarily mean that the microscopic Hamiltonian of the system has three modes, for the same reasons as above. On the other hand, the number of modes seen at zero external field (where all crystallites are equivalent) are directly relevant to the Hamiltonian, as we will discuss later.

The low temperature ESR was further explored by far infrared spectroscopic methods. The advantage of detecting ESR by far-IR spectroscopy is that one can readily map the power absorption over the full range of magnetic fields and

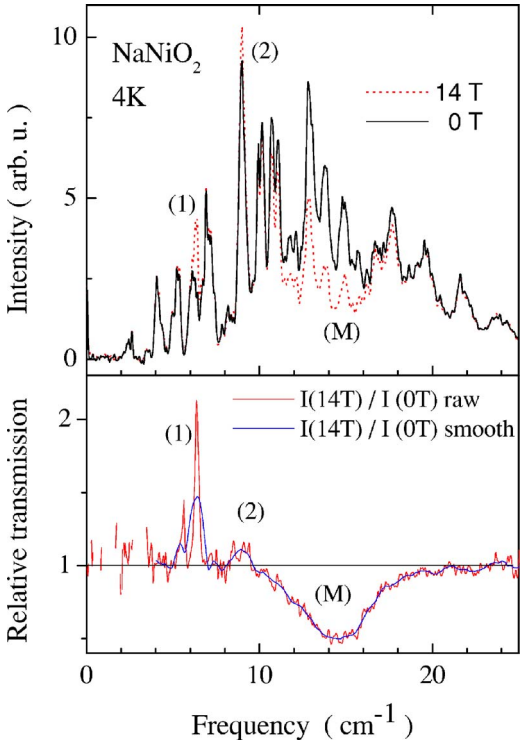

FIG. 2. (Color online) Upper part: Typical FT-ESR spectra recorded at 4 K, 0 T and 14 T. Lower part: relative transmission.

frequencies. The measurement does not rely on sweeping the magnetic field; this becomes especially important when one tries to discern features at zero field, or compare ESR to inelastic neutron scattering done in zero field.

Typical power spectra $I(H,\omega)$ recorded at $H=0$ and 14 T at 4 K in the frequency range $0<\omega<25$ cm^{-1} are given in Fig. 2. The sharp peaks in the spectra are "instrumental:" either due to interference features in the synchrotron source, or generated by the multiple reflections in the sample, or in the spectrometer itself. Nevertheless, the absorption due to spins is clearly visible with features around 6 cm^{-1} [labeled (1)], 9 cm^{-1} [labeled (2)], and 11–18 cm^{-1} [labeled (M)].

The key to these measurements is taking the ratio of two data sets at different fields, eliminating the features in the power spectrum of the incident light, and leaving only the field dependent part of the absorption due to the sample. We have chosen always the same procedure for the reference: the spectrum at zero field, taken just before or after the finite field measurements. With this procedure, we are able to extend the frequency range where reliable data are obtained down to 3 cm^{-1}. With this particular choice for the reference, the relative transmission data $T_r(H,\omega)$ is given by

$$T_r(H,\omega) = I(H,\omega)/I(0,\omega), \tag{1}$$

which depends only on the sample magnetic transmission $T_{\text{spin}}(H,\omega)$ so that

$$T_r(H,\omega) = T_{\text{spin}}(H,\omega)/T_{\text{spin}}(0,\omega). \tag{2}$$

An example of this procedure is given in Fig. 2 for $H=14$ T. An average over 3 to 4 data has been used to improve the signal to noise ratio, as well as a Fourier transform (FT) filter. The latter is responsible for the weak oscillations with the 2 cm^{-1} periodicity.

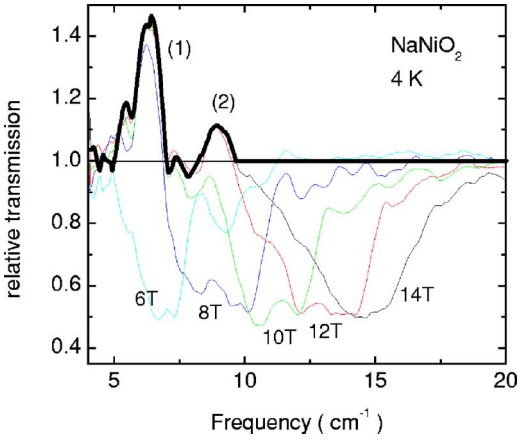

FIG. 3. (Color online) FT-ESR relative transmission $T_r(H,\omega)$ as a function of the electromagnetic wave frequency ω at different magnetic field values H. The thick black line gives an estimation of $1/T_{\text{spin}}(0,\omega)$ based on the data at 14 T below 10 cm^{-1}.

Several similar data obtained for magnetic fields up to 14 T are plotted in Fig. 3 for the frequency range 4–20 cm^{-1}. Below 10 cm^{-1} two broad peaks [(1) and (2)] lie above 1, indicating that the sample magnetic transmission at zero field, used as a reference, $T_{\text{spin}}(0,\omega)$, presents two resonance modes around 6 and 9 cm^{-1}. We assume no absorption below 10 cm^{-1} in the magnetic transmission at 14 T, i.e., we set $T_{\text{spin}}(14,\omega)=1$ and $1/T_{\text{spin}}(0,\omega)=T_r(14,\omega)$ for $\omega<10$ cm^{-1}, and use that to calculate the magnetic transmission at zero field [the solid black line in Fig. 3 represents $1/T_{\text{spin}}(0,\omega)$]. Then we deduced the sample magnetic transmission at finite field $T_{\text{spin}}(H,\omega)=T_r(H,\omega)\times T_{\text{spin}}(0,\omega)$ for each magnetic field value. We can map all these magnetic transmission spectra in a frequency/magnetic field diagram (Fig. 4). The color scale reflects the sample transmission intensity. We have also included the ESR results obtained by conventional ESR at fixed frequency (resonance line positions as in Fig. 1).

Several branches in the magnetic excitations are evident. The main branch (M) is a broad signal, with frequency approximately proportional to the field, significantly above the $g=2$ line. Modes (A) and (B) are related to the spin-flop transition observed at 1.8 T in the magnetization curve.[6] Mode (A) has been discussed previously in terms of an easy axis antiferromagnet model.[5] The field dependence of this mode is typical of crystallites in the powder where the static field is perpendicular to the easy axis. When the magnetic field is along the easy axis, a spin-flop transition occurs at 1.8 T. Crystallites oriented in this direction contribute to mode (B).

Modes (1) and (2) are seen mostly in the far-IR measurements, with supporting evidence from a field sweep at 225 GHz. These modes have very little field dependence. The corresponding zero field gaps are 6.5 and 9.0 cm^{-1}, respectively (0.85 and 1.1 meV). Mode (1) at 0.85 meV is close to the dispersionless magnon mode observed at

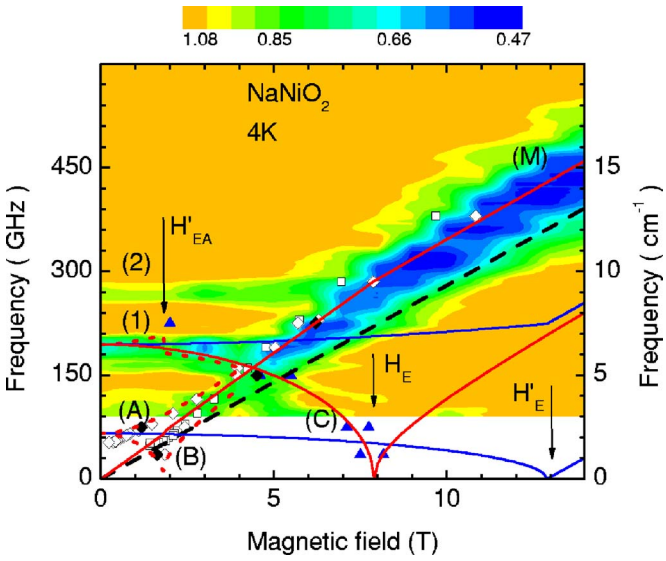

FIG. 4. (Color online) Magnetic modes at 4 K in a frequency versus field map obtained from the resonance lines positions in conventional ESR (closed symbols: this work; open symbols: from Ref. 5) and the transmission T_{spin} in FT-ESR (the color scale on the top refers to the intensity of the signal, as shown in Fig. 3). The dash black line corresponds to the paramagnetic resonance at $g=2$. The blue and red continuous lines represent the calculated frequencies $\omega^{\parallel}$ and $\omega^{\perp}$ corresponding to fields parallel and perpendicular to the hard axis, respectively. the red dotted lines ω^{int} are for fields along the intermediate axis (see Appendix B).

0.7 meV in inelastic neutron scattering measurements.[8] Mode (1) crosses the main branch, and appears again at low frequencies, labeled as mode (C), also seen in Fig. 1. Apparently, this mode softens to zero frequency around 8 T.

Further information can be deduced from a quantitative analysis of the FT-ESR data. We will assume that the sample transmission $T_{spin}(H,\omega)$ can be approximately related to the dissipative spin susceptibility χ'':

$$\ln T_{spin}(H,\omega) = \frac{-4\pi nd}{c}\chi''(H,\omega), \tag{3}$$

where c is the vacuum speed of light, n the refraction index, d is thickness of the sample, and ω the light frequency. The absorption peaks $\chi''(H,\omega)$ at fixed value of H are well fitted with a Gaussian line shape [see inset in Fig. 5(b)]. The corresponding resonance frequency, linewidth and total area are plotted as a function of the applied magnetic field [Figs. 5(a)–5(c), respectively]. Note that the line positions are unchanged whether one looks at $T_{spin}(H)$ or $\chi''(H)$. The line position and linewidth confirm that the resonance associated with the main branch (M) is nearly paramagnetic with $g \approx 2.2$. Its linewidth agrees with the linewidth calculated from the g anisotropy at 200 K. However, the anisotropic line shape observed at 200 K is no longer present here, presumably due to additional lifetime broadening. The branches (1) and (2) are clearly identified at 6.5 and 9 cm^{-1} with no field dependence until they both merge into the main branch (M).

The area under the absorption peak is related to the ESR susceptibility through the Kramers-Kronig relation

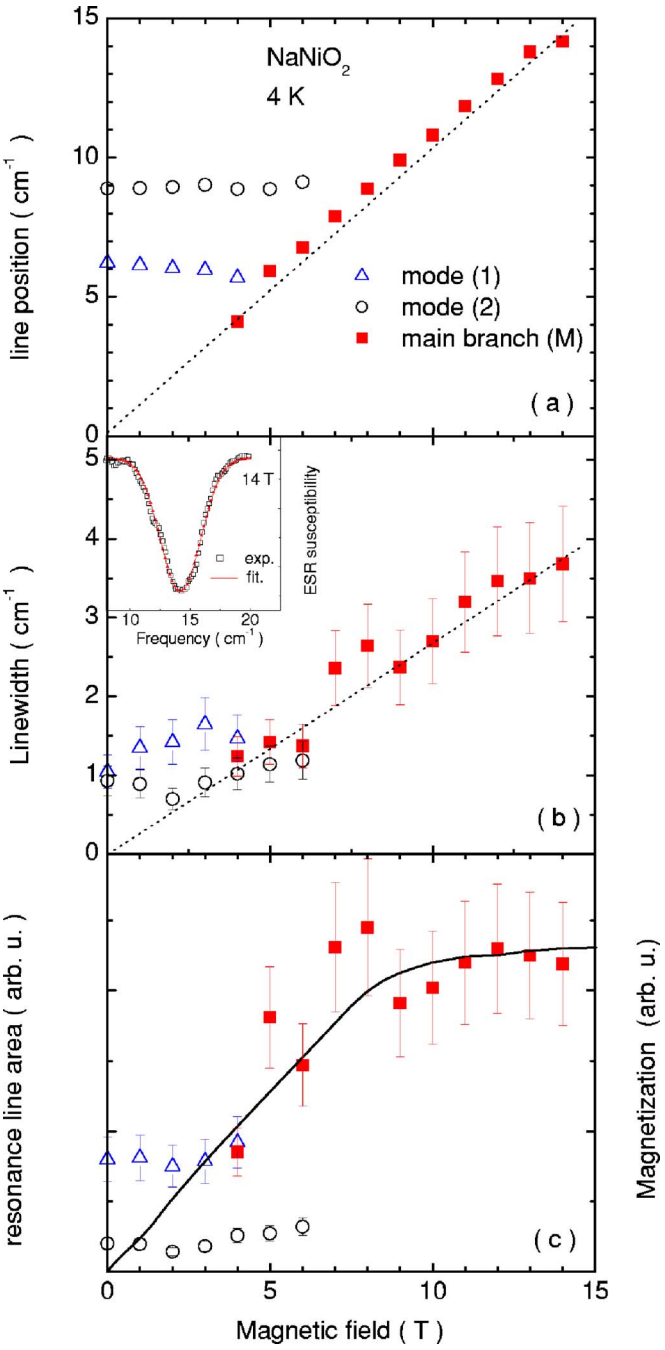

FIG. 5. (Color online) Gaussian fit of FT-ESR susceptibility at 4 K: line position (a), line width (b), and line total area (c) together with the sample magnetization (continuous line) as a function of applied magnetic field. The dotted line in (a) corresponds to the paramagnetic line at $g=2.2$ and in (b) to a g anisotropy linewidth $\Delta g=0.26$. Inset: Gaussian fit of the ESR susceptibility.

$$\chi'(H,0) \propto \int \frac{\chi''(H,\omega)}{\omega} d\omega \simeq \frac{1}{\omega_0}\int \chi''(H,\omega)d\omega, \tag{4}$$

where ω_0 is the peak position. For the main branch (M), ω_0 is proportional to the static field H. Then the peak area $\int\chi''(H,\omega)d\omega$ scales with the static magnetization. This is indeed observed in Fig. 5(c). The saturation of the total inten-

sity above 9 T is in accordance with the saturation of the static magnetization observed in this material.[9] For branches (1) and (2), ω_0 is constant. Then the peak area is proportional to the static susceptibility $\chi'(H,0)$. For both modes, it is constant with the field, as is expected away from spin-flop transitions. One can also see that mode (2) has a weaker susceptibility than mode (1). Note that this susceptibility measured on a powder sample includes the statistical weight associated with the crystallites which are oriented correctly relative to the magnetic field direction for each resonance mode.

These ESR results should be compared to the recent time-of-flight neutron inelastic measurements[8] performed on 30 g of powdered $NaNiO_2$. The two techniques should lead to the same mapping in frequency of the magnetic excitations when the magnetic field H is set to zero (ESR) and the wave vector Q tends to (0,0,0) (neutron). While three branches are observed in ESR, only two are visible in the neutron data. The main antiferromagnet (AF) branch which extrapolates to zero energy at (0,0,0) and at the magnetic zone center (0, 0, 1/2) corresponds to branch (A) in Fig. 4 with a finite gap of 0.22 meV. Such a small energy can only be detected in the conventional ESR measurements. The dispersionless branch around 0.7 meV corresponds to branch (1) in Figs. 4 and 3: it is centered at 6.5 cm^{-1}=0.81 meV. The discrepancy is within the uncertainty of the neutron results. The branch at 9 cm^{-1}=1.1 meV is 4 times weaker [Fig. 4(c)] and therefore cannot be detected by the neutron technique.

IV. DISCUSSION

Several models have been proposed to describe the magnetic properties in this material. The first one assumes a uniaxial easy axis antiferromagnet, proposed by Bongers *et al.*[6] to account for the spin-flop transition at 1.8 T and then used in Ref. 5 for the ESR magnon branch at 53 GHz [branch (A) in Fig. 4]. This model includes a strong ferromagnetic coupling in the Ni planes, a weaker antiferromagnetic coupling between the Ni planes and an even weaker anisotropy which aligns the spins in the easy axis direction. It was shown later that this model was incomplete in terms of explaining the magnetic properties, and an additional energy scale was required.[9] This conclusion was confirmed by the recent neutron inelastic scattering measurements.[8] The magnon spectrum was interpreted in terms of an easy plane AF model with the same ferromagnetic and antiferromagnetic couplings as in the previous model. The anisotropy was assigned to the ferromagnetic exchange coupling, and its magnitude was an order of magnitude larger than the weak anisotropy used in the evaluation of the ESR data.

These models were merged by assuming an anisotropy tensor that has an easy axis within an easy plane, with a much larger energy needed for turning the spins out of the plane than within the plane. This simple approach accounts for most of the experimental observations, including a better description of the low field ESR data of Chappel *et al.*[5] We start with the following anisotropic spin Hamiltonian:

$$\mathcal{H}_0 = \sum_{ab} \mathbf{S}_i \overleftrightarrow{J}_{ab} \mathbf{S}_j + \sum_{c} \mathbf{S}_i \overleftrightarrow{J}_{c} \mathbf{S}_j + g\mu_B \mathbf{S} \cdot \mathbf{H}, \qquad (5)$$

where $\mathbf{H}$ is the magnetic field, Σ_{ab} is over nearest neighbor spins within the layers, and Σ_c is over nearest neighbor spins along the c direction. The exchange interactions are represented by tensors: $\overleftrightarrow{J}_{ab}$ describes the ferromagnetic intraplane exchange, and $\overleftrightarrow{J}_{c}$ is the interplane antiferromagnetic exchange. The intensity and the frequency of the spin resonance lines for a crystal positioned in arbitrary direction relative to the external field can be calculated from the Hamiltonian in two steps. First, the spin configuration is determined by minimizing the free energy. Second, the ESR frequencies are related to the small oscillations around the equilibrium configuration. There are two resonance modes for any given field direction when the magnetic order is described by two sublattices. Occasionally (in zero field or field applied along high-symmetry directions) the two modes may be degenerate.

The powder spectrum is obtained by the average of the absorption of individual grains over all directions. In practice, the calculation of frequency and intensity for arbitrary field orientation is rather hard. Instead, the resonance frequency is calculated for the static field pointing in three principal directions. The six "principal frequencies" (three frequencies for each of the two modes) play a special role in the powder average, since some of them correspond to extremal values and the statistical weight factor for these frequencies will be high.

This process is similar to the determination of the $\overleftrightarrow{g}$ tensor from the paramagnetic resonance of a powder sample with a g-factor anisotropy. Naturally, the orientation of the principal axes of the tensor relative to the crystallographic directions cannot be determined from measurements on a powder sample. Nevertheless, the $\overleftrightarrow{g}$-tensor components are routinely determined from powder measurements this way. It is often sufficient to look at the highest and lowest frequencies in the measured broad ESR line, and one can identify the highest and lowest tensor components.

There is an extensive literature on the anisotropy effects in antiferromagnets, starting with the early work of Keffer and Kittel[12] on the easy axis problem. The three axis case (easy, intermediate, hard) was treated by Nagamiya.[13] Here we base our analysis on this work and on a review by Turov.[14] The magnon spectrum is treated in the linear approximation, equivalent to a quasiclassical treatment and we focus on the ground state properties (T=0 K). The details of the calculation are given in Appendixes A and B. First, the Hamiltonian is transformed into

$$\mathcal{H}_{\mathrm{MF}}/N = \frac{A}{2}\mathbf{m}^2 + \frac{a}{2}m_z^2 + \frac{b}{2}l_z^2 + \frac{c}{2}m_x^2 + \frac{d}{2}l_x^2 - \mathbf{m}\cdot\mathbf{h}, \qquad (6)$$

where $\mathbf{m}$ and $\mathbf{l}$ are the total magnetization and the antiferromagnetic order parameter, respectively, $\mathbf{m}=(\mathbf{m}_1+\mathbf{m}_2)$ and $\mathbf{l}=(\mathbf{m}_1-\mathbf{m}_2)$, with the dimensionless sublattice magnetizations $\mathbf{m}_1$ and $\mathbf{m}_1$ defined in Appendix A. Parameter A describes an isotropic antiferromagnetic coupling, a and c describe the anisotropy of the total ferromagnetic moment. Kittel treated the uniaxial model ($c=d=0$) at low fields; easy plane and easy axis corresponds to $b>0$ and $b<0$, respectively. Nagamiya's biaxial model is obtained when $a=c=0$. Turov discusses the uniaxial case for fields up to the saturation field.[14]

We set $b>0$ so that the zero field equilibrium magnetizations are in the plane perpendicular to z; this will be the "easy plane." The anisotropy within the plane, represented here by coefficients c and d, is much smaller: $c,d \ll b$. (Notice that these choices do not follow from the symmetry arguments related to the lattice distortion, but they were forced by the experimental observations.) Since c and d have similar effects on the spin resonance frequencies, and we cannot determine them separately, we will assume that $d=0$. This leaves us with four parameters to determine: A, a, b, and c. For $c<0$, x will be the easy direction, y will be the intermediate direction, and z remains the hard direction.

To facilitate the discussion, it is convenient to introduce the "effective fields" $H_E=A/M_0$, $H'_E=(A+a)/M_0$, and $H'_{EA}=\sqrt{Ac}/M_0$ where M_0 is the saturation magnetization (more effective fields follow in Appendix B). For applied field perpendicular to the hard axis the spin system saturates at H_E, when the external field overcomes the exchange field. For applied field parallel to the hard axis the saturation occurs at H'_E.[14] There is a spin-flop transition for field along the easy axis at $H=H'_{EA}$.[13]

The published susceptibility data, Fig. 4 of Ref. 9 can be used to find all but one of the parameters of the model. The first peak in the dM/dH curve at 1.8 T has been already identified as the spin-flop field H'_{EA}.[5] At around 8 T the dM/dH curve has a shoulder. We identify this as the onset of the saturation, and the corresponding field is H_E. Finally, the saturation is complete around 13 T, corresponding H'_E. From these values we get $A=8$ T, $a=5$ T, and $c=-0.42$ T.

The parameter b determines the ESR frequency ω_2 at zero field. We selected $b=6$ T to match the zero field gap at 6.5 cm^{-1} [mode (1) in Figs. 4 and 5]. This is quite close to the dispersionless magnon mode seen in neutron scattering (0.7 meV=5.6 cm^{-1}).[8]

The principal frequencies are listed in Appendix B, and the results are shown in Fig. 4. Considering that many of the parameters of the model were taken from other measurements, the agreement with the experiment is excellent. The calculated zero field resonance ω_1^{hard} is very close to the measured one at 53 GHz.[5] In fact, the low field behavior of our model (where the slope $d\omega/dH$ is zero for $H\to 0$) fits the lower branch in Fig. 8 of Ref. 5 better than the uniaxial easy axis model used in that work (where the $d\omega/dH=-\gamma$). Mode (1) is identified with ω_2. As the field is increased, this mode is approximately independent of the field for any field direction. Therefore the powder signal remains narrow, and it is clearly visible in the fixed-field far-IR spectroscopy scans.

Field-independent modes, such as the ω_2^{hard} and ω_2^{int} modes here, are very hard to detect in the field-sweep scan commonly used with the fixed-frequency methods. However, the spin-flop transition that occurs in the part of the sample where the field is close to the easy direction causes a jump in the frequency of ω_2^{easy}. This jump creates a measurable signal in the field-sweep scan.[13] In our case the 225 GHz fixed frequency ESR measurement was just in the right frequency range to catch this feature.

Above 5 T the powder average signal originating from ω_2 broadens and merges with other absorption. It cannot be seen in the far-IR measurement, and only the (more sensitive) fixed frequency study picks it up as mode (C). The upper extremum of all possible frequencies $\omega_1^{\perp}$ yields a strong signal. Although the g-factor was not adjusted ($g=2$), the coefficient $\sqrt{1+H_a/H_E}$ seen in Eq. (B2) brings $\omega_1^{\perp}$ right into the middle of the experimental values of the main branch (M).

With the set of parameters $A=8$ T, $a=5$ T, $b=6$ T, and $c=-0.42$ T, we can deduce the coupling energies in the Hamiltonian described by Eq. (5). For the antiferromagnetic coupling we get $J^z_{\text{AF}}=A/3=3.58$ K. The anisotropy of the ferromagnetic interaction is $J^z_F-J^y_F=(a+b)/3=4.93$ K, comparable to the antiferromagnetic coupling. The anisotropy of the antiferromagnetic coupling is weak $J^z_{\text{AF}}-J^y_{\text{AF}}=(a-b)/3=0.45$ K. The ferromagnetic coupling, deduced from the Curie-Weiss temperature $J^z_F=-15$ K, is the dominant interaction. This hierarchy of interactions was also deduced from inelastic neutron scattering by Lewis *et al.*[8] using a similar model.

The weak anisotropy within the easy plane can be assigned to the ferromagnetic or antiferromagnetic couplings or a combination of the two. The parameter c represents the sum of the two anisotropies $2c/3=(J^x_F-J^z_F)-(J^y_F-J^z_F)+(J^x_{\text{AF}}-J^z_{\text{AF}})-(J^y_{\text{AF}}-J^z_{\text{AF}})=-0.37$ K. However, the measurements would be compatible with other combinations of these parameters (as long as the sum is fixed). For example, all anisotropy may be in the ferromagnetic coupling $(J^x_F-J^z_F)-(J^y_F-J^z_F)=-0.37$ K and no anisotropy in the antiferromagnetic coupling $(J^x_{\text{AF}}-J^z_{\text{AF}})-(J^y_{\text{AF}}-J^z_{\text{AF}})=0$.

We tested the model with various other choice of parameters, partially disregarding the three characteristic fields obtained from the susceptibility measurements. Decreasing a to zero fails to describe the flatness of mode (1). Negative values of a do not give good fits. For $a=b$ the agreement with the data is still reasonable; in this special case the uniaxial anisotropy of the antiferromagnetic interplane coupling $J^z_{\text{AF}}-J^y_{\text{AF}}$ is exactly zero.

In spite of the general agreement between the model and the experiment, there are two features that remain unexplained: the splitting of mode (C) at low temperature (Fig. 1, inset) and the existence of mode (2). The splitting in mode (C) is consistent with our model. This mode is detected when the field is perpendicular to the hard axis. Note that the calculations for $\omega_2^{\perp}$ were done with $c=0$, but in the presence of a finite c the saturation field may be slightly different for static fields along the easy and intermediate axes. The magnitude of parameter $|c|=0.42$ T is in the right range to explain the observed splitting.

The existence of mode (2) is entirely beyond the simple model presented here. The two-sublattice Hamiltonian yields two modes at zero field, and we have those two modes identified as mode (A) at 1.75 cm^{-1} (53 GHz) and mode (1) at 6.5 cm^{-1}. No room is left for mode (2) in this model.

V. CONCLUSION

We studied the field dependence of the ESR in $NaNiO_2$ and we interpreted the results in terms of a model involving anisotropic exchange interactions. The main interaction is ferromagnetic in the triangular NiO plane. It is an order of

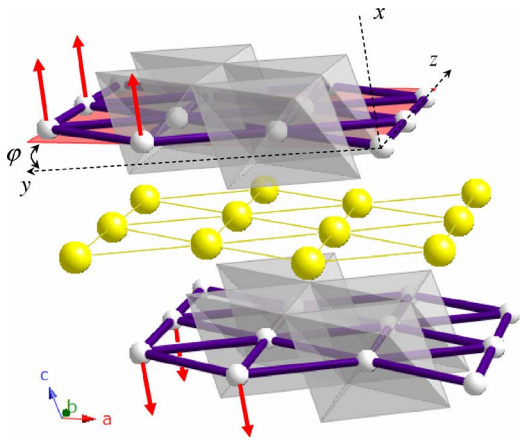

FIG. 6. (Color online) The orientation of the hard axis z and the easy axis x relative to the triangular Ni layers. The ab plane is highlighted in the top layer. The z axis is parallel to the b direction in the crystal; the angle between the ab plane and the y axis is $\varphi \approx 10°$. The spin directions are indicated by red arrows.

magnitude larger than the interplane antiferromagnetic coupling. The anisotropy in the ferromagnetic coupling is characterized by an uniaxial "easy plane" parameter of $a+b=11$ T, and a much weaker easy axis parameter of $c=-0.42$ T.

One of the main results of our work is that the easy direction is only slightly better than the other directions perpendicular to the hard axis. This is in general agreement with the inelastic neutron scattering result, where the magnon spectrum was modeled with an easy plane spin Hamiltonian.[8] For the easy plane system one of the magnon modes has zero energy (in zero field and at zero wavenumber). The anisotropy within the easy plane pushes this magnon mode to a finite energy ($1.8\ \mathrm{cm}^{-1}=0.2$ meV). This second magnon gap is small, and therefore it is not visible in the neutron scattering, but it is clearly seen in the ESR studies.

The principal axes of the anisotropy tensor were constrained by symmetry considerations (see Appendix A), but cannot be determined uniquely. In order to reconcile our results with the magnetization measurements on a twinned crystal[6] and with the neutron diffraction results,[7] where the spin orientation was measured, the easy direction (the x axis of the reference frame) was selected so that it makes a 100° angle to the ab plane (see Fig. 6). The hard axis was selected within the triangular nickel plane, along the b direction of the crystal (Fig. 6). Alternatively, it may point in the y direction of the reference frame. The hard axis is probably related to spin-orbit effects on the ferromagnetic exchange. Indeed, the ratio $|(J_F^z-J_F^y)/J_F^y|=0.33$ is comparable to the spin-orbit effect on the g tensor $(g^{\perp}-g^{\parallel})/g^{\parallel}=0.10$. The choice of the easy axis involves an energy scale one order of magnitude smaller.

The existence of a third zero-field mode (mode 2) may point beyond the model used here: any two-sublattice model, that assumes that the magnitude of the sublattice magnetizations are fixed, yields at most two resonance modes in zero field. One can then think of quantum effects. They may cause some modes to shift from zero to finite frequencies,[16] but do not change the number of modes. The comparison with other triangular magnets having antiferromagnetic coupling *within* the layers is intriguing: [including $CsNiBr_3$, $RbNiBr_3$, $CsMnI_3$, $CsMnBr_3$, $CsCuCl_3$, $RbCuCl_3$, and $RbFe(MoO_4)_2$]. There, typically three or six ESR modes[16–18] are observed. This is related to the umbrellalike spin order with, for a given triangle, each spin pointing at 120° from each other. Three sublattices are definitely present. This is not supposed to be the case in $NaNiO_2$ where there is strong support that the coupling within the triangular layers is ferromagnetic (the Curie-Weiss temperature is positive and the neutron diffraction patterns correspond to an A-type antiferromagnet with ferromagnetically aligned spins in the layers[7]). However, the sign of the interactions in the triangular planes has been the subject of intense debate in the isomorphic compound $LiNiO_2$.[2] Even for $NaNiO_2$ a recent calculation by Vernay *et al.*[3] proposes that one out of three interactions bond in the triangles are antiferromagnetic leading to antiferromagnetic chains, although this magnetic structure has not been observed experimentally. More over, in the intermediate compound $Li_{0.3}Na_{0.7}NiO_2$,[9] which, in the orbital sector, behaves as $LiNiO_2$ with no long range orbital order and, in the spin sector, presents a long range antiferromagnetic order as in $NaNiO_2$, we also observe the occurrence of three modes at zero field (around 0, 5.2, and 6.5 cm^{-1}); there the magnetic structure has not been solved yet. It is tempting to assign these similar behaviors to the presence of additional antiferromagnetic interactions. Further studies, preferably on single crystals, may solve this remaining puzzle in the $NaNiO_2/LiNiO_2$ layered triangular compounds.

ACKNOWLEDGMENTS

We are indebted to G.L. Carr for valuable discussions and for developing the IR facilities at the NSLS and F. Mila, F. Vernay, C. Lacroix, and M.D. Núñez-Regueiro for their theoretical inputs. S.B. acknowledges the Université Joseph Fourier for a CRTC program. The Budapest authors acknowledge the Hungarian State Grants No. (OTKA) TS049881, No. T60984, and No. F61733, and Grant No. MERG-CT-2005-022103 EU Project. F.S. acknowledges the Magyary program for support. L.M. acknowledges the Szent-Györgyi program. The Grenoble High Magnetic Field Laboratory is "laboratoire Conventionnée à L'Université Joseph Fourier." Use of the National Synchrotron Light Source, Brookhaven National Laboratory, was supported by the U.S. Department of Energy, Office of Science, Office of Basic Energy Sciences, under Contract No. DE-AC02-98CH10886.

APPENDIX A: DERIVATION OF THE MEAN FIELD HAMILTONIAN AND SYMMETRIES

In the molecular field approximation the spins are assigned to two sublattices: Spins in the even layers are labeled by μ and spins in the odd layers are labeled by ν. $\mathbf{S}_i$ and $\mathbf{S}_j$ in the Hamiltonian are replaced with their average values,

$\mathbf{S}_1=2/N\Sigma\mathbf{S}_\mu$ and $\mathbf{S}_2=2/N\Sigma\mathbf{S}_\nu$, where N is the total number of spins.

First, let us look at the term $\Sigma_{ab}\mathbf{S}_i\vec{J}_{ab}\mathbf{S}_j$ in the Hamiltonian (5). All of the spins in this sum belong to the same sublattice, so the terms to add up will have the form of $\mathbf{S}_1\vec{J}_{ab}\mathbf{S}_1$ and $\mathbf{S}_2\vec{J}_{ab}\mathbf{S}_2$. For any given spin within a ferromagnetic layer, there are six neighbors, approximately positioned on the corners of a hexagon. Even though the exchange $\vec{J}_{ab}$ with any one of this neighbors may be anisotropic, in the sum of the six terms most of the anisotropy within the plane will be cancelled. In fact, as long as the exchange couplings can be represented by tensors, in an undistorted lattice the cancellation will be exact. The corresponding part of the Hamiltonian would be $\Sigma_{ab}\mathbf{S}_i\vec{J}_{ab}\mathbf{S}_j=(N/2)(1/2)6(\mathbf{S}_1\vec{J}_F\mathbf{S}_1+\mathbf{S}_2\vec{J}_F\mathbf{S}_2)$, where the effective coupling $\vec{J}_F$ is isotropic within the plane, the extra factor of $1/2$ compensates for the double counting of each bond and the factor 6 reminds us that this exchange is an average over six bonds. Similar arguments can be used for the antiferromagnetic interlayer coupling to derive $\vec{J}_{\mathrm{AF}}$ from a sum over $\vec{J}_c$'s. The proper reference frame for the new coupling tensors has the x direction perpendicular to the layers. The (equivalent) y and z directions are within the layers.

The anisotropy of the effective couplings $\vec{J}_F$ and $\vec{J}_{\mathrm{AF}}$ is related to the distortion of the lattice. While above 480 K all nearest neighbor Ni-Ni bond lengths are equal,[4] below the transition one side of the triangular lattice (along the b direction) is compressed, and two other sides are elongated. The a-c plane remains a mirror plane, but the direction perpendicular to the layers is not a high symmetry direction anymore (see Fig. 6). Accordingly, the x direction will tilt relative to the direction perpendicular to the layers, as it acquires a nonzero component in the crystallographic a direction. At the same time the anisotropy axes within the plane become well defined. We will take the z axis parallel to the b crystallographic direction. The y axis will point slightly out of the plane, being perpendicular x and z. Notice that, except for permutations of the x,y,z labels, this is the only selection satisfying the broken crystal symmetries. The magnitude of the tilt of the x axis, and the amount of anisotropy, remain a free parameters. Similar arguments apply to the nearest neighbor antiferromagnetic coupling between the layers.

Spin resonance on a powder sample can be used to evaluate the anisotropy parameters of the resonance line. As we will see later, our system is described by a model with a dominant "easy plane" anisotropy, and a much weaker anisotropy within the plane. However, the orientation of the anisotropy axes relative to the crystal cannot be determined from a powder measurement. Neutron diffraction[7] and single crystal magnetization data[6] indicate that the easy axis makes an angle of approximately 100° to the NiO planes. We select this to coincide with the easy direction (the x axis of the reference frame). The hard axis may be either along y or z; both choices agree with existing symmetries. We tentatively pick the z direction for the hard axis.

The mean field Hamiltonian becomes

$$\mathcal{H}_{\mathrm{MF}}=\frac{3N}{2}[J_F^x(S_{1x}^2+S_{2x}^2)+J_F^y(S_{1y}^2+S_{2y}^2)+J_F^z(S_{1z}^2+S_{2z}^2)]+3N(J_{\mathrm{AF}}^xS_{1x}S_{2x}+J_{\mathrm{AF}}^yS_{1y}S_{2y}^2+J_{\mathrm{AF}}^zS_{1z}S_{2z}^2)+\frac{N}{2}g\mu_B(\mathbf{S}_1+\mathbf{S}_2)\mathbf{H}. \tag{A1}$$

The dimensionless sublattice magnetizations are defined as $\mathbf{m}_1=\frac{1}{2}\mathbf{S}_1/S$ and $\mathbf{m}_2=\frac{1}{2}\mathbf{S}_2/S$. When thermal and quantum fluctuations are neglected, the length of these vectors is fixed $|\mathbf{m}_1|=|\mathbf{m}_2|=1/2$. Accordingly, we can express one of the sublattice magnetization components with the other two: $m_{1z}^2=1/4-m_{1x}^2-m_{1y}^2$ and $m_{2z}^2=1/4-m_{2x}^2-m_{2y}^2$. The Hamiltonian is

$$\mathcal{H}_{\mathrm{MF}}=12NS^2[(J_F^x-J_F^z)(m_{1x}^2+m_{2x}^2)+(J_F^y-J_F^z)(m_{1y}^2+m_{2y}^2)]+6NS^2(J_{\mathrm{AF}}^xm_{1x}m_{2x}+J_{\mathrm{AF}}^ym_{1y}m_{2y}+J_{\mathrm{AF}}^zm_{1z}m_{2z})+NSg\mu_B(\mathbf{m}_1+\mathbf{m}_2)\mathbf{H}, \tag{A2}$$

and we dropped a constant term proportional to J_F^z. In the absence of fluctuations the magnitude of the ferromagnetic coupling becomes irrelevant, only the anisotropy matters. Interestingly, the anisotropy term obtained here for the ferromagnetic coupling cannot be distinguished (within the molecular field approximation) from a microscopic "single ion" spin anisotropy. However, the physical origins are different: For spin $1/2$ the microscopic single ion anisotropy can be shown to be exactly zero, whereas the same arguments do not apply here, where the anisotropy is due to the ferromagnetic exchange coupling.

The easy plane anisotropy around the z axis corresponds to $(J_F^x-J_F^z)\approx(J_F^y-J_F^z)$ (and similarly for the antiferromagnetic coupling). We can rearrange the terms to better reflect this fact. For m_1 we get

$$\begin{aligned}(J_F^x-J_F^z)m_{1x}^2+(J_F^y-J_F^z)m_{1y}^2&=1/2[(J_F^x-J_F^z)+(J_F^y-J_F^z)](m_{1x}^2+m_{1y}^2)\\&\quad+1/2[(J_F^x-J_F^z)-(J_F^y-J_F^z)](m_{1x}^2-m_{1y}^2)\\&=1/2[(J_F^x-J_F^z)+(J_F^y-J_F^z)](1-m_{1z}^2)\\&\quad+1/2[(J_F^x-J_F^z)-(J_F^y-J_F^z)](2m_{1x}^2-1+m_{1z}^2)\\&=(J_F^z-J_F^y)m_{1z}^2+[(J_F^x-J_F^z)-(J_F^y-J_F^z)]m_{1x}^2+\mathrm{const.}\end{aligned} \tag{A3}$$

This way the coefficient of the m_{1z}^2 term represents the uniaxial anisotropy; the (smaller) coefficient of the m_{1x}^2 term describes the remaining anisotropy around the z axis. Similar rearrangement can be made for m_2 and for all of the antiferromagnetic terms.

The total magnetization and the antiferromagnetic order parameter vectors are introduced as $\mathbf{m}=(\mathbf{m}_1+\mathbf{m}_2)$ and $\mathbf{l}=(\mathbf{m}_1-\mathbf{m}_2)$. Notice that $|\mathbf{m}|=1$ corresponds to the saturation magnetization, and $|\mathbf{l}|=1$ describes perfect antiferromagnetic order. In terms of these new parameters the Hamiltonian can be rewritten as

$$\mathcal{H}_{\mathrm{MF}} = 3NS^2[J^z_{\mathrm{AF}}(\mathbf{m}^2 - \mathbf{l}^2) + (J^z_{\mathrm{AF}} - J^y_{\mathrm{AF}})(m_z^2 - l_z^2) + (J^x_{\mathrm{AF}} - J^z_{\mathrm{AF}}) - (J^y_{\mathrm{AF}} - J^z_{\mathrm{AF}})(m_x^2 - l_x^2) + (J^z_F - J^y_F)(m_z^2 + l_z^2)] + [(J^x_F - J^z_F) - (J^y_F - J^z_F)(m_x^2 + l_x^2)] + Ng\mu_B \mathbf{m}\cdot\mathbf{H}. \quad \text{(A4)}$$

Here we regrouped the terms in the antiferromagnetic coupling, emphasizing the anisotropy, without introducing new constraints. Neglecting fluctuations leads to $\mathbf{m}\cdot\mathbf{l}=0$ and $\mathbf{m}^2+\mathbf{l}^2=1$. Eliminating the $\mathbf{l}^2$ term finally yields

$$\mathcal{H}_{\mathrm{MF}}/N = \frac{A}{2}\mathbf{m}^2 + \frac{a}{2}m_z^2 + \frac{b}{2}l_z^2 + \frac{c}{2}m_x^2 + \frac{d}{2}l_x^2 - \mathbf{m}\cdot\mathbf{h}, \quad \text{(A5)}$$

where $A=12S^2J^z_{\mathrm{AF}}$, $\mathbf{h}=g\mu_B S\mathbf{H}$, and the anisotropy constants are expressed as

$$a = 6S^2(J^z_F - J^y_F + J^z_{\mathrm{AF}} - J^y_{\mathrm{AF}}), \quad b = 6S^2(J^z_F - J^y_F - J^z_{\mathrm{AF}} + J^y_{\mathrm{AF}}),$$

$$c = 6S^2[(J^x_F - J^z_F) - (J^y_F - J^z_F) + (J^x_{\mathrm{AF}} - J^z_{\mathrm{AF}}) - (J^y_{\mathrm{AF}} - J^z_{\mathrm{AF}})],$$

$$d = 6S^2[(J^x_F - J^z_F) - (J^y_F - J^z_F) - (J^x_{\mathrm{AF}} - J^z_{\mathrm{AF}}) + (J^y_{\mathrm{AF}} - J^z_{\mathrm{AF}})]. \quad \text{(A6)}$$

Notice that Eq. (A5) is applicable in the most general case, but the coupling constants reflect an expected hierarchy. A simple isotropic antiferromagnet is obtained for $a=b=c=d=0$. For uniaxial anisotropy $c=d=0$; the coefficients a and b describe anisotropies in the total magnetization and antiferromagnetic order, respectively. In our case coefficients c and d will be small.

APPENDIX B: SPIN RESONANCE FREQUENCIES

For any given field direction there are two modes, denoted by ω_1 and ω_2. At high external fields one can neglect the small anisotropy within the easy plane, and take $c=d=0$. The frequencies were determined by Turov.[14] There are two principal frequencies for each modes, corresponding to external field applied parallel and perpendicular to the hard axis. The results are expressed in terms of effective fields

$$H_E = A/M_0,$$

$$H'_E = (A+a)/M_0,$$

$$H''_E = (A-b)/M_0,$$

$$H_a = a/M_0,$$

$$H_b = b/M_0,$$

$$H_{EA} = \sqrt{H_E H_b},$$

$$H_{\parallel} = \sqrt{H''_E H_b},$$

$$H_{\perp} = H_{\parallel}\frac{H'_E}{H''_E}, \quad \text{(B1)}$$

where M_0 is the saturation magnetization.

For field perpendicular to the hard axis one gets

$$\omega_1^{\perp} = \gamma H\sqrt{1 + H_a/H_E} \quad \text{if} \quad H < H_E,$$

$$\omega_1^{\perp} = \gamma\sqrt{H(H+H_a)} \quad \text{if} \quad H > H_E,$$

and

$$\omega_2^{\perp} = \gamma H_{EA}\sqrt{1 - H^2/H_E^2} \quad \text{if} \quad H < H_E,$$

$$\omega_2^{\perp} = \gamma\sqrt{(H - H''_E)(H - H_E)} \quad \text{if} \quad H > H_E, \quad \text{(B2)}$$

where $\gamma=g\mu_B/\hbar$ in terms of the Bohr magneton and the g factor. H_E is the saturation field; for $H>H_E$ all spins line up with the external field.

For the field direction parallel to the hard axis the saturation field is $H'_E>H_E$, since both the exchange coupling and the anisotropy work against the external field. The frequencies are

$$\omega_1^{\parallel} = 0 \quad \text{if} \quad H < H'_E,$$

$$\omega_1^{\parallel} = \gamma(H - H'_E) \quad \text{if} \quad H > H'_E,$$

and

$$\omega_2^{\parallel} = \gamma H_{EA}\sqrt{1 + H^2/H_{\perp}^2} \quad \text{if} \quad H < H'_E,$$

$$\omega_2^{\parallel} = \gamma(H - H_a) \quad \text{if} \quad H > H'_E. \quad \text{(B3)}$$

The modes are shown in the high field part of Fig. 4. The $\omega_2^{\perp}$ mode reaches zero at the lower saturation field H_E. Below the saturation field the $\omega_1^{\perp}$ mode looks similar to "free" spin resonance, except for the apparent g factor is increased by a factor of $\sqrt{1+H_a/H_E}$. Well above the saturation field the line is shifted to higher frequencies by the amount of $\gamma H_a/2$, but its slope is still γ. For fields parallel to the hard axis the $\omega_1^{\parallel}$ mode is zero at the upper saturation field. For the particular choice of parameters indicated in Fig. 4, the $\omega_2^{\parallel}$ mode is nearly independent of the field up to H'_E.

At low fields the anisotropy within the easy plane becomes important. A finite value of the parameter c (or d) has two important consequences. First, in zero field, the ω_1 mode (the "Goldstone mode") will shift to finite frequency. Second, the field dependence of the $\omega_1^{\perp}$ mode will be different for external fields applied in different directions within the easy plane. Instead of the two principal directions relative to the hard axis z (parallel and perpendicular), we will have to deal with three axes. We will identify these directions as the hard axis (parallel to z), the intermediate axis and the easy axis (formerly the two equivalent directions perpendicular to z).

For an approximate treatment of the $c\neq 0$ case we will turn to an early paper by Nagamiya,[13] assuming $H \ll H_E$. In finite fields along the hard axis the ω_1 mode is approximately independent of the field (this mode corresponds to the rotation of the spins in the easy plane, and it is excited with an

oscillating magnetic field parallel to the static field). For fields in the intermediate direction the frequency of the mode increases; for the field applied in the easy direction there will be a spin-flop transition at $H=H'_{EA}=\sqrt{Ac}/M_0$

$$\omega_1^{\text{hard}} = \gamma' H'_{EA} = \omega_1^{\parallel},$$

$$\omega_1^{\text{int}} = \gamma' \sqrt{H^2 + H'^2_{EA}},$$

$$\omega_1^{\text{easy}} = \gamma' \sqrt{\frac{\alpha}{2} + H^2 - \sqrt{\beta^2/4 + 2\alpha H^2}} \quad \text{if} \quad H < H'_{EA},$$

$$\omega_1^{\text{easy}} = \gamma' \sqrt{H^2 - H'^2_{EA}} \quad \text{if} \quad H > H'_{EA}. \tag{B4}$$

Here, we used $\alpha=H_{EA}^2+H_{EA}'^2$ and $\beta=H_{EA}^2-H_{EA}'^2$. Nagamiya's calculation does not account for the increase of the apparent g factor seen in Turov's low field result. Therefore, we are using a modified $\gamma'=\gamma\sqrt{1+H_a/H_E}$ here.

The anisotropy within the easy plane has no influence on the $\omega_2^{\parallel}$ mode (for fields parallel to the hard axis). For fields applied in the intermediate direction, the ω_2 mode is approximately independent of the field (except for a slight decrease in frequency, a precursor of the eventual saturation at H_E). When the field is in the easy direction, the spin-flop transition results in a jump of the ESR frequency:

$$\omega_2^{\text{hard}} = \gamma H_{EA},$$

$$\omega_2^{\text{int}} = \gamma H_{EA},$$

$$\omega_2^{\text{easy}} = \gamma \sqrt{\frac{\alpha}{2} + H^2 + \sqrt{\beta^2/4 + 2\alpha H^2}} \quad \text{if} \quad H < H'_{EA},$$

$$\omega_2^{\text{easy}} = \gamma \sqrt{H_{EA}^2 - H'^2_{EA}} \quad \text{if} \quad H > H'_{EA}. \tag{B5}$$

To ensure a seamless match to the high field calculation, in Fig. 4 we multiplied these frequencies with a saturation term $\sqrt{1-H^2/H_E^2}$. For the hard axis direction we used the original $\omega_2^{\parallel}$ values. Neither this procedure, nor the modified γ' introduced earlier, can completely substitute for the full solution of the problem for arbitrary fields and parameters, but they are qualitatively correct.

*Present address: Paul-Scherrer-Institut, CH-5232 Villigen PSI, Switzerland.

[1] For a review, see M. F. Collins and O. A. Petrenko, Can. J. Phys. **75**, 605 (1997).

[2] Y. Kitaoka, T. Kobayashi, A. Koda, H. Wakabayashi, Y. Niino, H. Yamakage, S. Taguchi, K. Amaya, K. Yamaura, M. Takano, A. Hirano, and R. Kanno, J. Phys. Soc. Jpn. **67**, 3703 (1998); F. Reynaud, D. Mertz, F. Celestini, J. M. Debierre, A. M. Ghorayeb, P. Simon, A. Stepanov, J. Voiron, and C. Delmas, Phys. Rev. Lett. **86**, 3638 (2001); E. Chappel, M. D. Núñez-Regueiro, S. de Brion, G. Chouteau, V. Bianchi, D. Caurant, and N. Baffier, Phys. Rev. B **66**, 132412 (2002).

[3] M. D. Núñez-Regueiro, E. Chappel, G. Chouteau, and C. Delmas, Eur. Phys. J. B **16**, 37 (2000); M. V. Mostovoy and D. I. Khomskii, Phys. Rev. Lett. **89**, 227203 (2002); F. Vernay, K. Penc, P. Fazekas, and F. Mila, Phys. Rev. B **70**, 014428 (2004); A. J. W. Reitsma, L. F. Feiner, and A. M. Olés, New J. Phys. **7**, 121 (2005).

[4] E. Chappel, M. D. Núñez-Regueiro, G. Chouteau, O. Isnard, and C. Darie, Eur. Phys. J. B **17**, 615 (2000).

[5] E. Chappel, M. D. Núñez-Regueiro, F. Dupont, G. Chouteau, C. Darie, and A. Sulpice, Eur. Phys. J. B **17**, 609 (2000).

[6] P. F. Bongers and U. Enz, Solid State Commun. **4**, 153 (1966).

[7] C. Darie, P. Bordet, S. de Brion, M. Holzapfel, O. Isnard, A. Lecchi, J. E. Lorenzo, and E. Suard, Eur. Phys. J. B **43**, 159 (2005).

[8] M. J. Lewis, B. D. Gaulin, L. Filion, C. Kallin, A. J. Berlinsky, H. A. Dabkowska, Y. Qiu, and J. R. D. Copley, Phys. Rev. B **72**, 014408 (2005).

[9] M. Holzapfel, S. de Brion, C. Darie, P. Bordet, E. Chappel, G. Chouteau, P. Strobel, A. Sulpice, and M. D. Núñez-Regueiro, Phys. Rev. B **70**, 132410 (2004).

[10] D. Talbayev, Ph.D. thesis, Stony Brook University, Stony Brook, 2004.

[11] D. Talbayev, L. Mihaly, and J. Zhou, Phys. Rev. Lett. **93**, 017202 (2004); L. Mihaly, D. Talbayev, L. F. Kiss, J. Zhou, T. Feher, and A. Janossy, Phys. Rev. B **69**, 024414 (2004).

[12] F. Keffer and C. Kittel, Phys. Rev. **85**, 329 (1952).

[13] T. Nagamiya, Prog. Theor. Phys. **11**, 309 (1954).

[14] E. A. Turov, *Physical Properties of Magnetically Ordered Crystals* (Academinc Press, New York, 1965).

[15] S. de Brion *et al.* (unpublished).

[16] A. V. Chubukov and D. I. Golosov, J. Phys.: Condens. Matter **3**, 69 (1991).

[17] L. E. Svistov, A. I. Smirnov, L. A. Prozorova, O. A. Petrenko, L. N. Demianets, and A. Ya. Shapiro, Phys. Rev. B **67**, 094434 (2003).

[18] H. Tanaka, T. Ono, S. Maruyama, S. Teraoka, K. Nagata, H. Ohta, S. Okubo, S. Kimura, T. Kambe, H. Nojiri, and M. Motokawa, J. Phys. Soc. Jpn. **72**, 84 (2003).